BULLETIN DE L'ASSOCIATION MINÉRALOGIQUE DU CANADA

THE CANADIAN MINERALOGIST

JOURNAL OF THE MINERALOGICAL ASSOCIATION OF CANADA

Volume 40 December 2002 Part 6

The Canadian Mineralogist
Vol. 40, pp. 1553-1569 (2002)

U AND Pb ISOTOPE ANALYSIS OF URANIUM MINERALS BY ION MICROPROBE AND THE GEOCHRONOLOGY OF THE McARTHUR RIVER AND SUE ZONE URANIUM DEPOSITS, SASKATCHEWAN, CANADA

MOSTAFA FAYEK[§]

Department of Geological Sciences, 306 Geology Building, The University of Tennessee, Knoxville, Tennessee 37996, and Oak Ridge National Laboratory, P.O. Box 2008, Oak Ridge, Tennessee 37831, U.S.A.

T. KURTIS KYSER

Department of Geological Sciences, Queen's University, Kingston, Ontario K7L 3N6, Canada

LEE R. RICIPUTI

Oak Ridge National Laboratory, P.O. Box 2008, Oak Ridge, Tennessee 37831, U.S.A.

ABSTRACT

A method for *in situ* U–Pb isotopic analyses by secondary ion mass spectrometry (SIMS) has been developed for uranium minerals with a range of chemical compositions. This method combines the advantages of conventional U–Pb dating (*i.e.*, use of concordia) and *in situ* analysis, and therefore is ideally suited for the study of chemically complex and fine-grained uranium oxides associated with uranium deposits. An ion-yield normalizing coefficient (αSIMS) that accounts for variation in relative ion-yields with chemical composition of the mineral of interest was calculated using uraninite standards that cover a range of U and Pb compositions, and an appropriate empirical mass-bias model was developed. The coefficient αSIMS varies as a function of wt% PbO, requiring two working curves to define the relationship between the $^{206}Pb^+/^{238}U^+$ and $^{207}Pb^+/^{235}U^+$ values measured by SIMS *versus* the "true" $^{206}Pb/^{238}U$ and $^{207}Pb/^{235}U$ values:

$$^{207}Pb^+/^{235}U = 0.762 \pm 0.015\ (^{207}Pb^+/^{235}U^+)^{0.69\pm0.02}$$

$$^{206}Pb/^{238}U = 0.333 \pm 0.007\ (^{206}Pb^+/^{238}U^+)^{0.64\pm0.02}$$

The application of this technique to unconformity-type uranium deposits in the Athabasca Basin, Saskatchewan, demonstrates that at the microscale, these deposits preserve the initial age of mineralization (1486 to 1519 Ma) and a temporal record of accretion and breakup of supercontinents. Prior to *in situ* analyses, this detailed chronological record was obscured by the wide variability in U–Pb and Pb–Pb data obtained by micro-drilling and conventional isotopic analyses due to mixing of different generations of minerals.

Keywords: uraninite, U–Pb, SIMS analyses, ages, geochronology, fluid-circulation events, Athabasca Basin, Saskatchewan.

[§] E-mail addresses: mfayek@utk.edu, kyser@geol.queensu.ca, i79@ornl.gov

SOMMAIRE

Nous avons développé une méthode d'analyser *in situ* les minéraux d'uranium à composition chimique variable afin d'en obtenir ponctuellement les rapports isotopiques U–Pb. La méthode, qui fait appel à la spectrométrie de masse des ions secondaires (SIMS), possède les avantages d'une datation conventionnelle U–Pb (utilisation des diagrammes concordia) et d'une analyse *in situ*, et serait donc idéale pour l'analyse des oxydes complexes d'uranium, à granulométrie fine, associés aux gisements d'uranium. Un coefficient normalisateur décrivant l'efficacité de production des ions (αSIMS) rend compte des variations en production relative dépendant de la composition chimique du minéral analysé; il a été calculé à partir des étalons d'uraninite représentatifs d'un intervalle de concentrations en U et Pb, et comprend un modèle empirique approprié servant à corriger un biais massique. Le coefficient αSIMS varie en fonction de la proportion de PbO, et requiert deux fonctions afin de définir la relation entre les valeurs de $^{206}Pb^+/^{238}U^+$ et $^{207}Pb^+/^{235}U^+$ mesurées par analyses SIMS *versus* les "vraies" valeurs de $^{206}Pb/^{238}U$ and $^{207}Pb/^{235}U$:

$$^{207}Pb^+/^{235}U = 0.762 \pm 0.015\ (^{207}Pb^+/^{235}U^+)^{0.69\pm0.02}$$

$$^{206}Pb/^{238}U = 0.333 \pm 0.007\ (^{206}Pb^+/^{238}U^+)^{0.64\pm0.02}$$

L'application de cette approche aux gisements discordants d'uranium du bassin d'Athabasca, au Saskatchewan, démontre qu'à un échelle microscopique, ces gisements conservent l'âge initial de minéralisation (1486 à 1519 Ma) et un bilan temporel de l'accrétion et du démembrement des supercontinents. Avant cette possibilité de faire des analyses *in situ*, la résolution chronologique des événements majeurs était impossible à cause de la grande variabilité en données U–Pb et Pb–Pb disponibles par micro-carottage et analyses isotopiques conventionnelles, due au mélange de différentes générations de minéraux.

(Traduit par la Rédaction)

Mots-clés: uraninite, U–Pb, analyses SIMS, âges, géochronologie, événements de circulation des fluides, bassin d'Athabasca, Saskatchewan.

INTRODUCTION

Secondary ionization mass spectrometry (SIMS) is a technique that provides *in situ* measurement of isotopic ratios with a spatial resolution on the scale of a few μm. The ion microprobe has been used for over 30 years to measure the U–Pb isotope systematics of minerals (*e.g.*, Anderson & Hinthorne 1972, Holliger 1988, Williams *et al.* 1996). The ability to obtain precise measurements of an isotope ratio from individual grains has improved U–Pb geochronological results on zircon (*e.g.*, Meyer *et al.* 1996) and uranium-rich minerals (Meddaugh 1983, Holliger 1988, 1991, Cathelineau *et al.* 1990, Fayek *et al.* 2000).

Recent studies of the Cigar Lake deposit have demonstrated the utility of using a combination of SIMS and electron probe to study the chronology of complex uranium-rich minerals (Fayek *et al.* 2000, 2002). These and other studies demonstrate that the U–Pb isotope systematics of uranium-rich minerals from the Cigar Lake deposits have been affected paleo-fluid-flow events that were controlled by regional and global-scale tectonic events (Kotzer & Kyser 1995, Kyser 2000, Kyser *et al.* 2000). In this study, we have developed a robust method for U–Pb dating of uranium-rich minerals by ion microprobe; the method does not require the use of an electron probe. This method is here applied to uranium minerals from other unconformity-type uranium deposit from the Athabasca Basin as an extension of the work conducted on the Cigar Lake deposit. The SIMS technique combines the advantages of conventional U–Pb dating (*i.e.*, use of concordia) and *in situ* analysis. This method thus is ideally suited for the study of chemically and mineralogically complex and fine-grained uranium oxides associated with unconformity-type uranium deposits.

SECONDARY ION MASS SPECTROMETRY

A SIMS analysis requires a focused beam of primary ions a few μm in diameter, which bombards the solid surface of a sample to carry out a localized analysis. The bombardment or "sputtering" removes atoms from the polished surface of the specimen. Some of these atoms are ionized during the process, and can be focused and accelerated as a "secondary" beam through a slit and into a mass spectrometer (Reed 1989). For U and Pb measurements, a 12.5 keV O^- primary beam is used because it enhances the yield of secondary positive ions (*e.g.*, U^+, Pb^+, Th^+).

During the measurement process, a mass-dependent bias, referred to as instrumental mass fractionation (IMF), is introduced, and it typically favors the light isotope. The observed IMF results from a variety of processes, including secondary atom ionization (sputtering) and extraction (*e.g.*, Sigmund 1969, Schroeer *et al.* 1973, Williams 1979, Yu & Lang 1986), secondary ion transmission (*e.g.*, Shimizu & Hart 1982), and detection (*e.g.*, Lyon *et al.* 1994, Riciputi *et al.* 1998). Sputtering and ionization, which depend strongly upon sample characteristics (*i.e.*, chemical composition), are the greatest contributors to variability in IMF. Therefore, accurate isotopic analysis by SIMS requires calibration using a mineral standard that is compositionally similar to the unknown to correct for IMF. Ion-microprobe results from the standard are compared to its accepted isotopic composition in order to calculate a correction factor that is applied to the unknowns measured during the same analytical session (*e.g.*, Holliger 1988, Cathelineau *et al.* 1990, Meyer *et al.* 1996).

Quite commonly, the minerals of interest (*e.g.*, magnesite, siderite) vary considerably in their chemical composition or are chemically zoned at the micrometer scale, and it is impractical to find standards that match the wide range in chemical compositions of the unknowns. Therefore, a mass-bias model that accounts for variation in IMF with chemical composition for the minerals of interest is necessary. These models are developed using a suite of standards with chemical compositions that cover the range of compositions of the unknowns where a working calibration curve is developed (*e.g.*, Riciputi *et al.* 1998). In addition, the relative ion-yields of two elements and their isotopes, such as U and Pb, may vary as function of chemical composition, producing erroneous measurements of elemental and isotopic ratios. For example, the $^{206}Pb^{+}/^{238}U^{+}$ value measured by SIMS may deviate significantly from the "true" $^{206}Pb/^{238}U$ value because Pb ionizes more readily than U. In addition, the $^{206}Pb^{+}/^{238}U^{+}$ value also may vary as a function of chemical composition of the sample because other elements present (*i.e.*, Si, Ca) may enhance the ion-yield of Pb^{+} or U^{+}. Therefore, an ion-yield normalizing coefficient (αSIMS) that accounts for variation in relative ion-yields with chemical composition for the mineral of interest is necessary (Holliger 1991, Cathelineau *et al.* 1990). Similarly, models are developed using a suite of standards with chemical compositions that cover the range of compositions of the unknowns, and a working calibration curve is developed (Riciputi *et al.* 1998).

PREVIOUS ION-MICROPROBE STUDIES OF URANIUM OXIDE MINERALS

Previous ion-microprobe investigations of the U–Pb isotope systematics of U-oxide minerals (Meddaugh 1983, Fourel *et al.* 1988, Holliger 1988, 1991, 1994, Holliger & Cathelineau 1986, 1987, 1988, Cathelineau *et al.* 1990, Fayek *et al.* 2002, Evins *et al.* 2001) have revealed important information regarding the formation history of certain types of uranium deposits, but were limited in adaptability and accuracy by possible matrix-effects and the requirement of a uraninite standard homogeneous in Pb/U.

Holliger (1988) characterized a sample of uraninite from Vendée, France, for use as an ion-microprobe standard. The U–Pb isotopic composition (*i.e.*, $^{206}Pb/^{238}U$) of this material was characterized by microdrilling thin sections and analyzing the extracted material by thermal ionization mass spectrometry. Five measurements gave a concordant age of 540 Ma. Using an 8 keV Ar^{+} primary ion beam focussed to a 10 μm spot, Holliger (1988) found Pb^{+} and UO_2^{+} ions to be the most abundant secondary ions of Pb and U. A normalizing coefficient, αSIMS, of 0.72 ± 0.02 (2σ), defined as the ratio of the true $^{206}Pb/^{238}U$ to the $^{206}Pb^{+}/^{270}UO_2^{+}$ value measured with the ion microprobe, was used to correct for ion-yield bias between Pb^{+} and UO_2^{+} (Holliger 1988). Holliger (1991) and Cathelineau *et al.* (1990) made use of another sample of uraninite from Vendée, which gave a concordant age of 285 Ma and exhibited homogeneous U and Pb concentrations over large regions (>200 μm). The Pb/U value of the sample was determined by electron microprobe, and this value was used to calculate a revised α value of 0.63 ± 0.03. Cathelineau *et al.* (1990) reported uncertainties in $^{206}Pb/^{238}U$, $^{207}Pb/^{235}U$, and $^{206}Pb/^{207}Pb$ values of 0.5%, 1%, and 0.08% (2σ), respectively.

A limitation of this technique is that the αSIMS value calculated for uraninite cannot be used to correct for ion-yield bias between Pb^{+} and UO_2^{+} ions in uraninite with U and Pb concentrations that differ significantly from the standard. In our own experience, relatively small differences in uraninite composition can significantly alter the relative efficiencies in ionization of these two species, essentially ruling out this approach for the complex compositions of naturally occurring uranium-bearing minerals (*e.g.*, Fayek & Kyser 1997, Fayek *et al.* 2002).

Meddaugh (1983) introduced a method later refined by Fayek *et al.* (2001) that utilizes both the electron and ion microprobes to obtain rapid and precise *in situ* U–Pb isotopic data on uranium minerals. With this technique, the Pb isotope ratios are determined by ion microprobe and the concentration of Pb is measured by electron probe. The results are combined to calculate the concentrations of ^{206}Pb and ^{207}Pb. Using the present-day $^{238}U/^{235}U$ value of 137.88, and the U concentration measured by electron microprobe, the amount of ^{238}U and ^{235}U is calculated. The concentrations of ^{238}U, ^{235}U, ^{206}Pb, and ^{207}Pb are then used to calculate $^{206}Pb/^{238}U$ and $^{207}Pb/^{235}U$ for each spot. This method avoids the need for a uraninite or coffinite ion-microprobe standard with a homogeneous Pb/U value because only the Pb isotopes are measured by ion microprobe, which exhibit negligible instrumental mass-fractionation (Meddaugh 1983, Evins *et al.* 2001). In addition, minor alteration-induced phases with complex chemistry, such as coffinite and Ca–U-rich phases, can be routinely analyzed for their U–Pb isotopic composition.

There are disadvantages to this technique: 1) each spot must be analyzed by both SIMS and electron microprobe, which lengthens the time of analysis, 2) the volume sampled by the electron beam is larger than the volume sampled by the ion beam, and 3) this method cannot be applied to samples that have experienced severe nuclear processes (such as the natural fission reactor zones at Oklo, Gabon), where the $^{238}U/^{235}U$ ratio departs from 137.88. The analytical approach used in this study combines both techniques to develop a series of equations, which relate normalizing coefficients (αSIMS) for U and Pb isotopic measurements by ion microprobe to chemical compositions (matrix effects).

ANALYTICAL CONDITIONS

Uraninite standards for SIMS analysis

The suite of uraninite samples used as SIMS U–Pb isotopic standards (Fig. 1) were examined for homogeneity and alteration by transmitted light microscopy, back-scattered electron imaging and quantitative electron-microprobe analysis. Chemical compositions of the uraninite standards (Table 1) were determined by wavelength-dispersion spectroscopy using an automated CAMECA SX50 X–ray microanalyzer operated at 15 keV, a beam diameter of 10 μm, and counting times of 40 s per element. Synthetic UO_2, grossular, and galena were used as standards for U, Si and Ca, and Pb, respectively. Detection limits of the elements were on the order of 0.1 wt%. The program PAP was used to reduce the data for the various elements. The oxygen contents

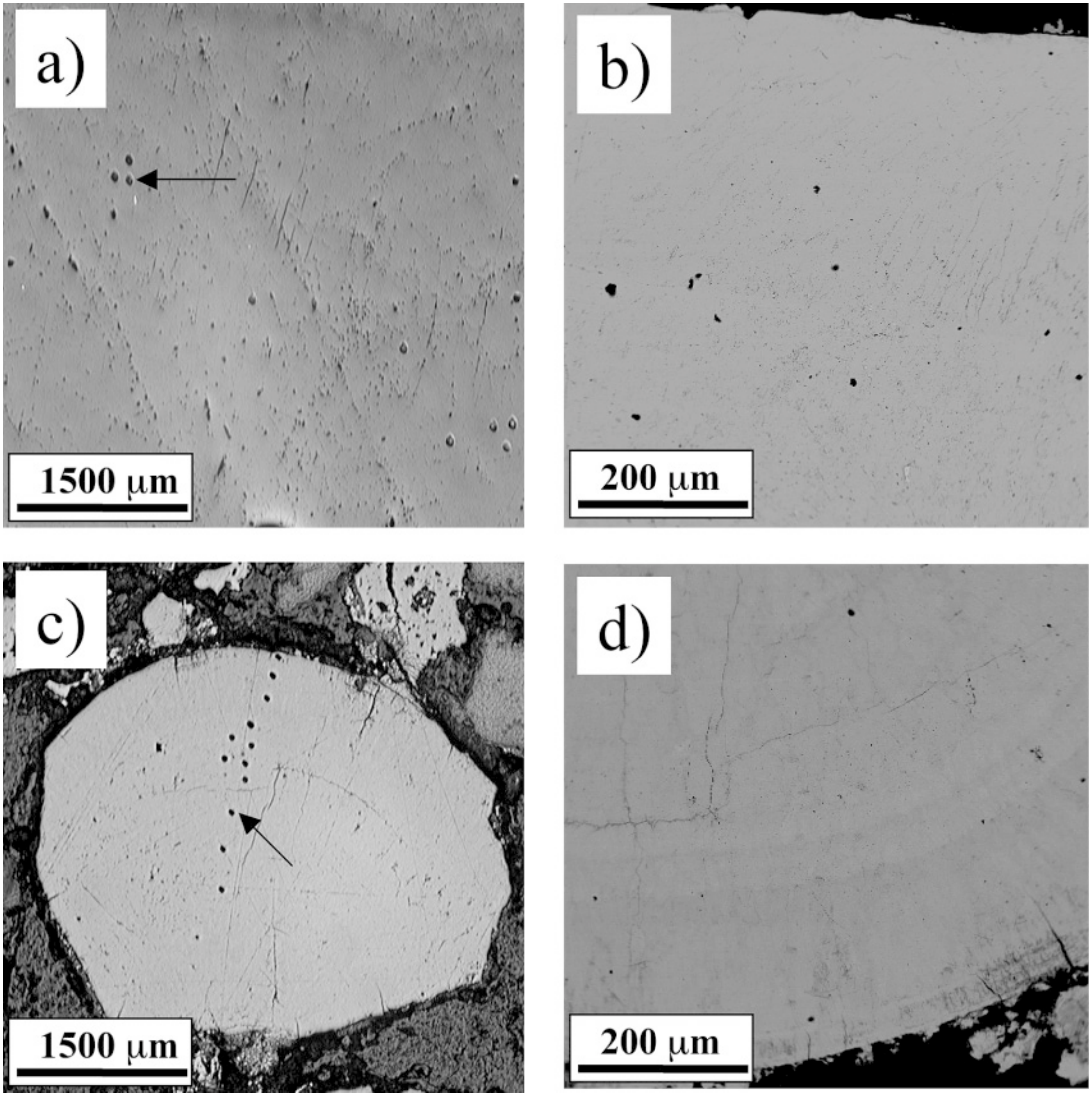

FIG. 1. (a) Reflected-light microscope image of the standard from the Topsham mine (TS), Main. (b) Back-scattered electron (BSE) image of the TS standard. (c) Reflected-light microscope image of a botryoid of uraninite from the Sue Zone (Sue 129), Athabasca Basin, which is used as a standard. (d) Back-scattered electron (BSE) image of Sue 129. Arrows point to ion-microprobe pits.

of uraninite were calculated by stoichiometry assuming an ideal composition of UO_2.

The standards were analyzed by ion microprobe to establish their U/Pb values, to verify that their U–Pb isotopic composition is homogeneous at the scale of the ion beam (*i.e.*, 10 μm). The small size of some standards (2 mm) precluded micro-drilling and U–Pb isotopic analysis by thermal ionization mass spectrometry (TIMS). Therefore, these standards were calibrated using the ion microprobe – electron microprobe technique, as described by Fayek *et al.* (2000, 2001), which is summarized below. However, the standard LAMNH 30222 was micro-drilled using a 100 μm diamond drill bit, and the powder separates were calibrated by TIMS (Evins *et al.* 2001).

U and Pb isotopic analyses of uranium oxides by ion microprobe

The analytical protocol for U–Pb measurements in uranium minerals using the CAMECA 4f is similar to that used for U–Pb analyses by Fayek *et al.* (2000). A ~2 nA primary ion beam of O^-, accelerated at 12.5 kV, was focused to a 15 × 30 μm spot using a 100 μm aperture in the primary column. The sample accelerating voltage was +4.45 kV, with electrostatic analyzer in the secondary column set to accept +4.5 kV. The entrance slit was narrowed to obtain flat-top peaks at a mass resolving power of about 500. Ions were detected with a Balzers SEV 1217 electron multiplier coupled with an ion-counting system with an overall deadtime of 15 ns. The following species were detected sequentially by switching the magnetic field: 203.5 (background), $^{204}Pb^+$, $^{206}Pb^+$, $^{207}Pb^+$, $^{208}Pb^+$, 209 ($^{208}Pb^+$ hydride), $^{235}U^+$, $^{238}U^+$, and 239 ($^{238}U^+$ hydride). During some analytical sessions, the $^{238}UO^+$ and $^{238}UO_2^+$ species were monitored in addition to the Pb and U ion species using a 0.5 nA primary beam.

The 50-volt energy offset in conjunction with a liquid nitrogen cold trap helped maintain a high vacuum ($1.5e^{-9}$ torr) in the sample chamber, and suppressed hydride isobaric interferences (Fig. 2). Mass scans indicate that isobaric interferences were negligible (Fig. 2). A typical analysis lasted ~10 minutes, comprising 25 cycles of analysis. Negligible amounts of common Pb ($^{204}Pb^+$) were detected.

The Pb isotope ratios from standards determined by ion microprobe and the concentration of Pb measured by electron microprobe were combined to calculate the concentrations of ^{206}Pb and ^{207}Pb. Using the $^{238}U/^{235}U$ value of 137.88 and the U concentration measured by electron microprobe, the amounts of ^{238}U and ^{235}U were calculated. The concentrations of ^{238}U, ^{235}U, ^{206}Pb, and ^{207}Pb were then used to calculate $^{206}Pb/^{238}U$ and $^{207}Pb/^{235}U$ for each spot. The equations used to calculate values of these ratios for the standards and error calculations are similar to those used by Fayek *et al.* (2000,

TABLE 1. ELECTRON-MICROPROBE DATA ON URANINITE STANDARDS

Sample	UO_2	PbO	SiO_2	CaO	FeO	ThO_2
Sue 129	75.1	16.3	0.04	1.31	0.11	0.04
Mc 503	77.8	14.4	0.12	0.89	0.30	0.02
Mc 515	81.1	9.9	0.36	1.26	0.40	0.04
LAMNH 30222	92.4	4.7	0.00	0.00	0.00	2.80
TS	82.0	3.1	0.00	0.09	0.02	7.48

All electron-microprobe data are reported in wt%. Uncertainty in measurents of the Pb and U concentrations is ±0.1 wt% (100 ppm). Abbreviations: Sue: Sue Zone, Mc: McArthur River, LAMNH: Los Angeles Museum of Natural History; TS: Topsham mine.

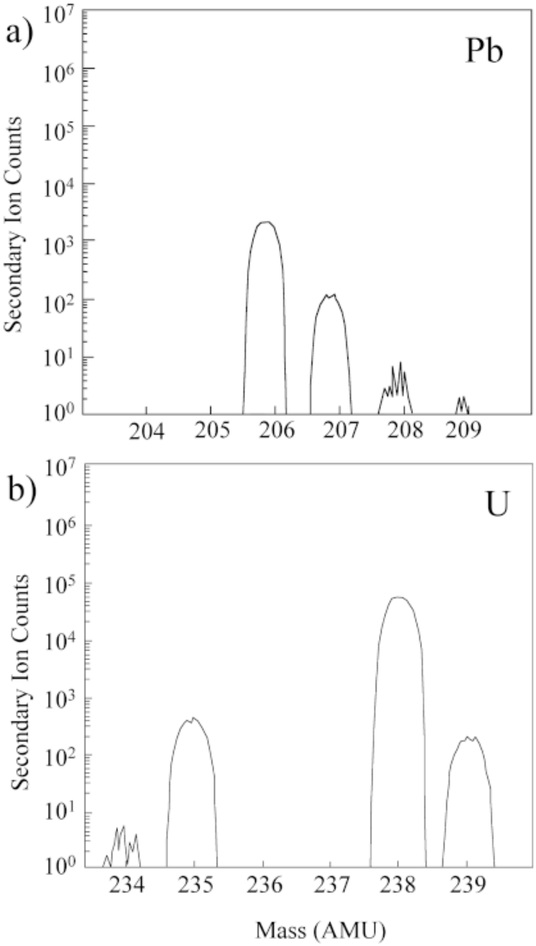

FIG. 2. Low-resolution (ΔM/M = 500) mass scans of (a) the lead isotopes and Pb-hydrides (mass 209) and (b) the uranium isotopes and U-hydrides (mass 239) in the standard LAMNH 30222.

2001). Concordia intersections were calculated using the program ISOPLOT (Ludwig 1993). Uncertainties in the ages are reported at the 2σ level in every case.

Preparation of samples from unconformity-type uranium deposits

Polished thin sections with uranium minerals from two unconformity-type uranium deposits from northern Saskatchewan, Canada, were cut into sections 25 mm diameter. The mounts were then washed with a dilute soap solution, rinsed in deionized water, dried and carbon coated. Uraninite, coffinite and Ca–U-rich phases were examined in the same way as the SIMS standards.

Prior to SIMS analysis, the mounts were re-polished, cleaned to remove the carbon coat, and reflected-light photomaps of the entire mount were made. A ~200 Å thick coat of gold was sputter-deposited on the surface of the sample mount prior to ion-microprobe analysis to ensure a surface conductivity of 5–10 ohms/cm. The mounts were placed in stainless steel sample holders, and the entire assembly was then placed in the ion-microprobe sample lock and held at high vacuum for a minimum of 8 hours prior to the start of the analysis.

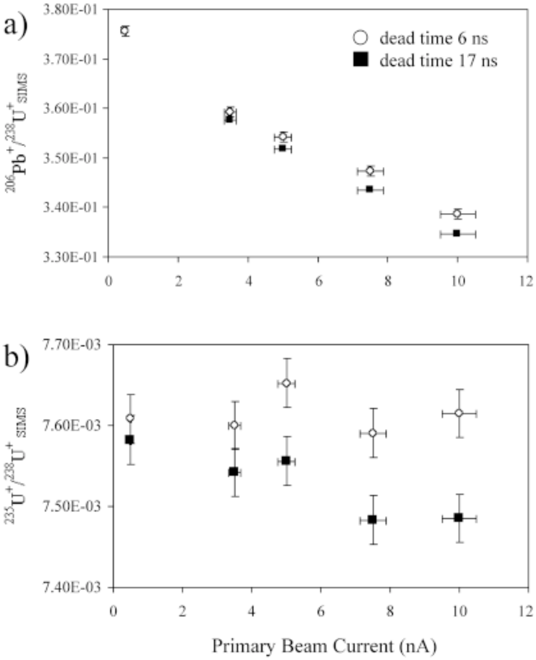

FIG. 3. (a) A plot of $^{206}Pb^+/^{238}U^+$ value measured by SIMS *versus* current of the primary beam, which shows that as the current is increased, the $^{206}Pb^+/^{238}U^+$ value decreases. (b) A plot of $^{235}U^+/^{238}U^+$ ratio measured by SIMS *versus* current of the primary beam similarly shows a decreasing $^{235}U^+/^{238}U^+$ value with increasing current. Although changing the dead time did affect the $^{235}U^+/^{238}U^+$ value obtained, it did not significantly affect $^{206}Pb^+/^{238}U^+$. Data are from Table 2.

RESULTS

Instrumental mass-fractionation

The instrumental mass-fractionation (IMF) for the isotopes of U and Pb was investigated by Evins *et al.* (2001). In summary, the fractionation factors for Pb isotopic analysis of uraninite obtained using the conditions described in the previous section and the CAMECA 4f at Oak Ridge National Laboratory (ORNL) indicate that the fractionation of Pb isotopes is approximately zero. However, this result differs from data collected using the CAMECA 1270 at the NORDSIM facility in Stockholm, Sweden, where the Pb isotopic fractionation was approximately 1%/*amu* in favor of the heavier Pb isotope. However, this value decreased during NORDSIM sessions once efforts were made to mimic the ORNL analytical conditions, such as using a cold trap, a 50 V offset, and placing the sample in vacuum prior to analyses (Evins *et al.* 2001). Therefore, these data indicate that hydrides were not completely resolved or sufficiently minimized at NORDSIM. Owing to the small amount of material that is sputtered, ^{204}Pb is virtually non-detectable. Therefore, the amount of common lead is negligible, and correction was not deemed necessary.

The fractionation factors for U isotopic analysis of uraninite are calculated by dividing the average result of each SIMS analytical session by the accepted value of $^{235}U/^{238}U$ (0.00725). The fractionation factor for U isotopes calculated from data collected at both ORNL and NORDSIM is 1.4 ± 0.1%/*amu* (1σ) and 1.4 ± 0.4%/*amu*, respectively, in favor of the lighter isotope (Evins *et al.* 2001).

TABLE 2. PRIMARY BEAM CURRENT AND ION-MICROPROBE DATA FOR STANDARD Mc 503

Beam (nA)	$^{206}Pb^+/^{238}U^+$ SIMS	2σ (%)	$^{235}U^+/^{238}U^+$ SIMS	2σ (%)
		Dead time = 17 ns		
0.5	3.76 E-01	0.3	7.58 E-03	0.5
3.5	3.58 E-01	0.3	7.54 E-03	0.5
5	3.52 E-01	0.3	7.56 E-03	0.5
7.5	3.44 E-01	0.3	7.48 E-03	0.5
10	3.35 E-01	0.3	7.49 E-03	0.5
		Dead time = 6 ns		
0.5	3.76 E-01	0.3	7.61 E-03	0.5
3.5	3.59 E-01	0.3	7.60 E-03	0.5
5	3.54 E-01	0.3	7.65 E-03	0.5
7.5	3.47 E-01	0.3	7.59 E-03	0.5
10	3.39 E-01	0.3	7.61 E-03	0.5

Inter-element fractionation

The secondary ion yield for a given element is related to the concentration of that element in the sputtered volume and a series of complex parameters such as the total sputtered yield per incident primary ion, ionization efficiency and the relative sputter efficiency of the element, and the extraction efficiency of the secondary ion optics for that element (Williams 1988, Williams 1998). All of these factors affect the measured inter-element value (*e.g.*, U/Pb) so that the measured value can be significantly different from the "true" value. Therefore, standards are required to correct for the difference between measured and "true" values.

We have investigated the inter-element fractionation of U and Pb as a function of primary ion beam current and spatially across a standard block. The results show that Pb/U decreases as the intensity of the primary beam increases (Fig. 3a, Table 2), whereas the $^{235}U/^{238}U$ value is not significantly affected by the change in the intensity of the primary beam (Fig. 3b, Table 2). Although this trend could be caused by an incorrect dead-time correction, changing the dead time did not significantly reduce the influence of the primary beam intensity (Figs. 4a, b). Therefore, for accurate Pb/U ratio analysis, it is critical to maintain a constant current for the primary beam. Traverses across large (1 × 0.8 cm) grains of the TS standards show that the Pb/U value does not change across isotopically homogeneous standards (Fig. 4).

U–Pb ion-yield normalizing coefficient (αSIMS): calculations and standardization

The ratios $^{206}Pb/^{238}U$ and $^{207}Pb/^{235}U$ measured for each standard by TIMS or the method described by Fayek *et al.* (2000, 2001) were compared to the $^{206}Pb^+/^{238}U^+$ and $^{207}Pb^+/^{235}U^+$ values obtained by SIMS (Table 3). Analysis sessions occurred over an 8-month period to check the reproducibility of the method (Table 3). An ion-yield normalizing coefficient (αSIMS), which is the ratio of the "true" values for $^{206}Pb/^{238}U$ and $^{207}Pb/^{235}U$ *versus* the values of $^{206}Pb^+/^{238}U^+$ and $^{207}Pb^+/^{235}U^+$ determined by SIMS, was calculated for each standard (Table 3). Values of αSIMS vary as a function of wt% PbO (Fig. 5a), and therefore two working curves were developed that define the relationship between the $^{206}Pb^+/^{238}U^+$ and $^{207}Pb^+/^{235}U^+$ values measured by SIMS *versus* the "true" $^{206}Pb/^{238}U$ and $^{207}Pb/^{235}U$ values (Figs. 6b, c):

$$y_1 = 0.762 \pm 0.015\ x_1^{0.69\pm0.02} \qquad [1]$$

$$y_2 = 0.333 \pm 0.007\ x_2^{0.64\pm0.02} \qquad [2]$$

where y_1 and y_2 are "true" values, and x_1 and x_2 are the values of $^{207}Pb^+/^{235}U^+$ and $^{206}Pb/^{238}U^+$, respectively, measured by SIMS. These equations were used to correct the $^{207}Pb^+/^{235}U^+$ and $^{206}Pb^+/^{238}U^+$ values obtained by SIMS for all the unknowns (Table 4), including

TABLE 3. ION-MICROPROBE DATA AND αSIMS FOR URANINITE STANDARDS

Sample	$^{207}Pb^+/^{206}Pb^+$ SIMS	error (%)	$^{208}Pb^+/^{206}Pb^+$ SIMS	error (%)	$^{207}Pb/^{235}U$ "True"	error (%)	$^{206}Pb/^{238}U$ "True"	error (%)	$^{207}Pb^+/^{235}U^+$ SIMS	error (%)	$^{206}Pb^+/^{238}U^+$ SIMS	error (%)	αSIMS $^{207}Pb/^{235}U$	error (%)	αSIMS $^{206}Pb/^{238}U$	error (%)	*n*
								2001									
Sue 129	0.08896	0.6	0.000804	2.5	2.586	1.8	0.211	1.8	5.418	2.0	0.460	2.0	0.48	2.0	0.46	2.0	9
Mc 503	0.08357	1.1	0.000173	2.1	2.087	1.7	0.181	1.7	4.253	2.0	0.384	2.0	0.47	2.0	0.45	2.0	6
LAMNH 30222	0.05421	2.6	0.002529	5.0	0.3788	1.7	0.0507	1.7	0.329	5.0	0.0457	5.0	1.15	5.0	1.11	5.0	6
LAMNH 30222	0.05381*	0.1	0.002607*	0.2	0.4105*	1.0	0.0554*	1.0	0.329	5.0	0.0457	5.0	1.25	5.0	1.21	5.0	
								2002									
Sue 129	0.08972	0.2	0.000334	2.0	2.607	0.9	0.211	0.9	5.541	2.0	0.463	2.0	0.47	2.0	0.46	2.0	5
Mc 503	0.08376	0.4	0.000189	2.1	2.091	1.1	0.181	1.1	4.222	2.0	0.377	2.0	0.50	2.0	0.48	2.0	5
Mc 515	0.06664	0.6	0.000121	2.2	1.115	1.5	0.121	1.5	2.134	5.0	0.241	5.0	0.52	5.0	0.50	5.0	10
TS A	0.05259	1.2	0.036833	0.5	0.2722	4.9	0.0375	4.9	0.284	5.0	0.0403	5.0	0.96	5.0	0.94	5.0	7
TS B	0.05295	2.0	0.031215	3.0	0.2722	4.9	0.0375	4.9	0.285	5.0	0.0402	5.0	0.96	5.0	0.93	5.0	4
TS C	0.05194	2.0	0.024221	3.0	0.2722	4.9	0.0375	4.9	0.273	5.0	0.0394	5.0	1.00	5.0	0.95	5.0	4

"True" values were calculated using the equations in Fayek *et al.* (2000) from results of electron-microprobe and SIMS analyses.

* Values measured by TIMS from Evins *et al.* (2001). Abbreviations: Sue: Sue Zone, Mc: McArthur River, LAMNH: Los Angeles Museum of Natural History; TS: Topsham mine. Errors are expressed as 2σ in all cases. *n*: number of analyses.

coffinite and Ca–U-rich phases. Although matrix effects were not extensively studied because of lack of suitable standards, the fact that coffinite and Ca–U-rich phases plot on concordia (see below) suggests that matrix effects are negligible, and that these equations can be used to correct the $^{207}Pb^+/^{235}U^+$ and $^{206}Pb^+/^{238}U^+$ values obtained by SIMS for uranium-rich minerals other than uraninite. However, Si- and Ca-rich uranium mineral standards such as coffinite and calciouranoite are required to adequately investigate the matrix effects on the U and Pb isotopic ratios, and on Pb/U values. In addition, grains of the TS standard were mounted on three separate blocks to determine the change in αSIMS between standard mounts. The data in Table 3 show that αSIMS does not change between standard mounts and, therefore, standards may be used to correct for unknowns mounted on separate mounts.

Several ion-microprobe studies of zircon and monazite have shown that Pb^+/U^+ varies as function of UO^+/U^+ (*e.g.*, Claoué-Long *et al.* 1995, Williams *et al.* 1996). Although there is a weak correlation between Pb^+/U^+ and the oxide species UO^+/U^+ (Fig. 6a) and UO_2^+/U^+ (Fig. 6b) for uraninite (Table 5), the large scatter in the data and the poor fit of the curve to the data suggest that this method is not an accurate technique of standardization for uraninite.

Although a detailed discussion of the formation of uranium oxide species during sputtering of uraninite is beyond the scope of this paper, a non-systematic formation of the uranium oxide species during sputtering may be due to oxygen occurring as structurally bound oxygen, bonded to uranium atoms, and as interstitial oxygen partially filling vacancies within the fluorite structure adopted by uraninite (Berman 1957, Fayek *et al.* 1997a). When the impinging primary beam implants oxygen into the uraninite structure, the implanted oxygen likely goes into these interstitial sites. Therefore, the interstitial oxygen is preferentially removed from the uraninite structure. However, because these vacancies in uraninite are only partially filled with oxygen, the amount of interstitial oxygen available to form oxide species and the degree of oxidation that occurs during sputtering likely depend on the proportion of vacancies that are filled.

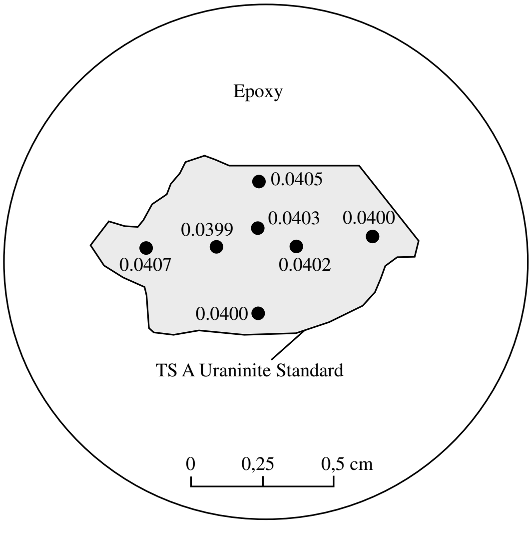

FIG. 4. A schematic representation of standard TS A from the Topsham mine, Maine. Shown are the location of the analyses and the $^{206}Pb^+/^{238}U^+$ values obtained.

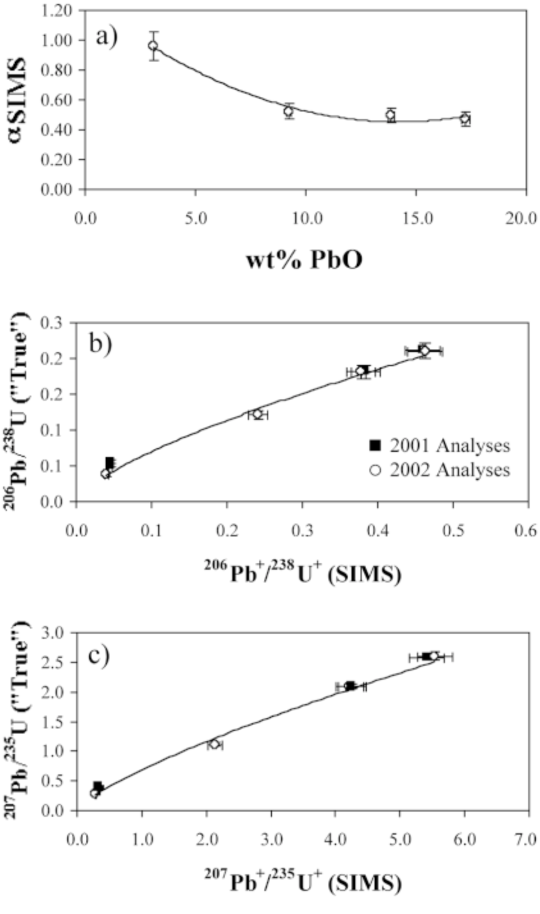

FIG. 5. A plot of (a) αSIMS for $^{207}Pb/^{235}U$ *versus* wt% PbO, (b) $^{205}Pb^+/^{237}U^+$ measured by SIMS *versus* $^{205}Pb/^{237}U$ ("true"), and (c) $^{206}Pb^+/^{238}U^+$ measured by SIMS *versus* $^{206}Pb/^{238}U$ ("true") for uraninite standards with different U and Pb concentrations. Data are from Table 3.

U–Pb Geochronology of Unconformity-Type Deposits

Geological considerations

The Athabasca Basin (Fig. 7) contains a sequence of Middle Proterozoic, mature quartz sandstones, collectively referred to as the Athabasca Group (Ramaekers 1981), that unconformably overlie Archean basement (MacDonald 1987). Deposition of uranium is generally interpreted to have occurred at moderate depths and temperatures (*ca*. 2–5 km and 200°C) in response to interaction of uraniferous, oxidizing, basinal brines with reducing basement-derived fluids along faults that crosscut the unconformity (Pagel *et al.* 1980, Kotzer & Kyser 1995).

Generally, high-grade uranium mineralization occurs as lenses of massive uraninite, the most common reduced (*i.e.*, U^{4+}) mineral containing uranium. However, subsequent infiltration of fluids has caused partial alteration of uraninite to uranyl silicate hydrate (coffinite) and uranyl oxide hydrate minerals (*e.g.*, Fayek & Kyser 1997, Fayek *et al.* 2002).

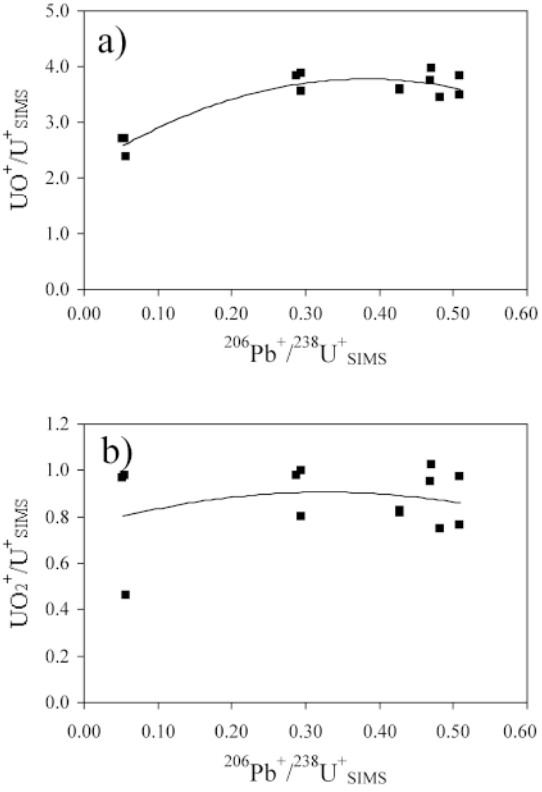

FIG. 6. (a) A plot of UO^+/U^+ measured by SIMS *versus* $^{206}Pb^+/^{238}U^+$ measured by SIMS, and (b) a plot of UO_2^+/U^+ measured by SIMS *versus* $^{206}Pb^+/^{238}U^+$ measured by SIMS, showing poor correlation between the U-oxide species and Pb–U ionic species. Data are from Table 5.

The paragenesis developed by Kotzer & Kyser (1993) and Fayek & Kyser (1997) was used to select uraninite samples that were categorized as stage-1, -2, and -3 uraninite based on cross-cutting relationships, textures observed in thin section and back-scattered electron images, oxygen isotopic composition, and chemical composition. Stage-1, -2 and -3 uraninite occurs as masses, cubes, and pseudo-cubes, ranging in size from 0.1 to 0.5 cm across. Stage-1 and -2 uraninite also occurs as nodular masses that attain a diameter of 5 mm and is characterized by high Pb contents (~15 and ~9 wt% PbO, respectively) and low Si and Ca contents (<3.5 wt% SiO_2, CaO), whereas stage-3 uranium minerals are characterized by low to moderate Pb contents (≤6 wt% PbO) and variable SiO_2 and CaO contents (Fayek & Kyser 1997, Fayek *et al.* 1997b). However, all three stages of uraninite have high uranium contents (~77 to ~85 wt% UO_2, Fayek & Kyser 1997, Fayek *et al.* 1997b). In thin section, Ca-rich uranyl oxide minerals are closely associated with coffinite and occur as homogeneous colloform bands along the edges of uraninite grains or as microveinlets that cut across uraninite grains (Fayek & Kyser 1997, Fayek *et al.* 1997b). Coffinite is characterized by low Pb contents (≤2 wt% PbO), moderate but variable Ca (0.42 to 4.94 wt% CaO) and occasionally low Si contents (9.00 to 18.41 wt% SiO_2, Fayek & Kyser 1997, Fayek *et al.* 1997b). Ca–U-rich minerals are characterized by low U contents (63.1 to 82.50 wt% UO_2), variable Pb contents (<0.1 to 12.17 wt% PbO), and intermediate to low Si and Ca contents (0.18 to 6.49 wt% SiO_2, CaO, Fayek & Kyser 1997, Fayek *et al.* 1997b). Rb/Sr dating of clay-mineral assemblages associated with each stage of uraninite formation (Kotzer & Kyser 1995) indicates that mineralization occurred at ~1500 Ma (stage 1), ~950 Ma (stage 2), and ~300 Ma (stage 3).

Considerable isotopic U–Pb, Pb–Pb, and chemical U–Pb dating has been performed in the Athabasca Basin to determine the timing of uranium mineralization. Analysis of uraninite samples generally gives highly discordant U–Pb ages between 1250 and 1525 Ma (*e.g.*, Cumming & Krstic 1992, Kotzer & Kyser 1993, Fayek & Kyser 1997), whereas secondary uranium minerals give much younger ages (*ca*. 200 Ma, Hoeve *et al.* 1985, Kotzer & Kyser 1993). Scattered results are obtained even where sampling is highly selective and involves mm-scale drilling of petrographic sections (*e.g.*, Cumming & Krstic 1992, Kotzer & Kyser 1993, Fayek & Kyser 1997). The wide range in both U–Pb and $^{207}Pb/^{206}Pb$, and in chemical Pb ages for each stage of uranium mineralization, has generally been attributed to variable alteration by fluids that facilitated preferential removal of Pb relative to U (*e.g.*, Kotzer & Kyser 1995, Fayek & Kyser 1997).

U–Pb and Pb–Pb isotope systematics

In the Athabasca uranium deposits, the ^{207}Pb/^{206}Pb ages of uraninite, coffinite and Ca-rich uranyl oxide minerals range from 1399 to 218 Ma (Table 4), with the entire range commonly encountered in a single thin section. High-reflectance samples tend to have homogeneous ^{207}Pb/^{206}Pb ages, with the majority of the ages ranging from 1399 to 1218 Ma (Table 4). They represent the earliest-formed uranium minerals. Samples with variable reflectance (Figs. 8a, b), imaged using back-scattered electrons, reveal multiple stages of mineral

TABLE 4. ION-MICROPROBE DATA FOR SAMPLES FROM THE SUE ZONE AND THE McARTHUR RIVER UNCONFORMITY-TYPE URANIUM DEPOSITS, ATHABASCA BASIN, SASKATCHEWAN

Sample DDH/ depth	Mineral	^{207}Pb$^+$/ ^{206}Pb$^+$ SIMS	error (%)	^{208}Pb$^+$/ ^{206}Pb$^+$ SIMS	error (%)	^{204}Pb$^+$/ ^{206}Pb$^+$ SIMS	error (%)	^{207}Pb/ ^{206}Pb Age (Ma)	^{207}Pb$^+$/ ^{235}U$^+$ SIMS	error (%)	^{206}Pb$^+$/ ^{238}U$^+$ SIMS	error (%)	^{207}Pb/ ^{235}U *corr.	error (%)	^{206}Pb/ ^{238}U *corr.	error (%)
Sue Zone																
528-129	Stage 1 Ur	0.08903	0.15	0.000631	2.8	0.000017	11.2	1387±4	5.564	1.1	0.474	0.8	2.535	2.0	0.207	2.0
528-129	Stage 1 Ur	0.08461	0.16	0.000238	7.3	0.000061	3.2	1283±5	3.666	0.8	0.327	0.6	1.893	2.0	0.163	2.0
528-129	Stage 1 Ur	0.08792	0.15	0.000754	2.3	0.000017	11.2	1361±4	5.268	1.1	0.450	0.8	2.440	2.0	0.200	2.0
528-129	Stage 1 Ur	0.08816	0.15	0.000631	2.8	0.000013	14.8	1367±4	4.931	1.0	0.424	0.7	2.329	2.0	0.193	2.0
528-129	Stage 1 Ur	0.08815	0.15	0.001521	1.1	0.000043	4.5	1367±4	4.926	1.0	0.423	0.7	2.328	2.0	0.192	2.0
528-129	Stage 1 Ur	0.08921	0.21	0.000508	1.8	0.000018	7.9	1391±6	5.614	0.4	0.475	0.4	2.551	2.0	0.207	2.0
528-129	Stage 1 Ur	0.08880	0.13	0.001008	0.9	0.000026	2.5	1382±4	5.274	0.7	0.449	0.5	2.442	2.0	0.200	2.0
528-129	Stage 1 Ur	0.08394	0.18	0.001652	2.4	0.000039	5.6	1267±5	3.238	1.1	0.293	0.5	1.735	2.0	0.152	2.0
528-129	Stage 1 Ur	0.08866	0.31	0.000935	1.2	0.000027	5.1	1378±9	5.209	0.9	0.442	0.4	2.420	2.0	0.198	2.0
528-129	Stage 1 Ur	0.08782	0.30	0.001601	1.1	0.000043	7.1	1359±9	4.974	0.7	0.426	0.4	2.344	2.0	0.193	2.0
528-129	Stage 1 Ur	0.08958	0.31	0.000547	1.4	0.000012	11.1	1399±9	5.192	0.7	0.439	0.2	2.415	2.0	0.197	2.0
528-129	Stage 1 Ur	0.08891	0.15	0.000989	1.0	0.000027	5.8	1384±4	5.673	0.7	0.481	0.3	2.569	2.0	0.209	2.0
528-129	Stage 1 Ur	0.08957	0.24	0.000653	1.9	0.000020	6.2	1399±7	5.540	0.6	0.467	0.2	2.527	2.0	0.205	2.0
528-129	Stage 1 Ur	0.08898	0.29	0.001214	0.9	0.000033	4.9	1386±8	5.428	0.5	0.460	0.3	2.491	2.0	0.203	2.0
528-129**	Stage 1 Ur	0.08194	0.16	0.000359	4.9	0.000010	20.3	1218±5	3.192	0.8	0.295	0.7	1.718	2.0	0.153	2.0
528-95	Stage 1 Ur	0.07569	0.36	0.000717	1.4	0.000016	6.9	1057±10	2.102	0.8	0.209	0.6	1.282	2.0	0.122	2.0
528-95	Stage 1 Ur	0.08008	0.30	0.000561	1.8	0.000013	6.7	1171±9	2.409	0.5	0.228	0.4	1.411	2.0	0.130	2.0
528-95	Stage 1 Ur	0.08782	0.30	0.001601	1.1	0.000043	7.1	1359±9	4.974	0.7	0.426	0.4	2.344	2.0	0.193	2.0
528-95	Stage 1 Ur	0.08130	0.30	0.000276	3.7	0.000007	12.8	1202±9	2.987	0.4	0.275	0.4	1.640	2.0	0.146	2.0
528-95	Stage 2 Ur	0.07406	0.24	0.000281	0.8	0.000008	13.9	1013±7	3.120	0.8	0.319	0.6	1.691	2.0	0.161	2.0
528-95**	Stage 2 Ur	0.07386	0.43	0.000440	3.6	0.000014	15.7	1007±12	1.177	0.9	0.119	0.6	0.855	2.0	0.086	2.0
528-95	Stage 2 Ur	0.07234	0.57	0.000551	2.3	0.000023	9.2	965±16	0.926	0.7	0.096	0.4	0.723	2.0	0.075	2.0
528-95	Stage 2 Ur	0.07112	0.44	0.000738	2.7	0.000021	12.1	930±13	1.137	1.1	0.121	1.1	0.834	2.0	0.086	2.0
528-95	Stage 2 Ur	0.07114	0.22	0.001029	1.4	0.000018	20.8	931±6	1.080	0.9	0.114	0.8	0.805	2.0	0.083	2.0
528-95**	Stage 2 Ur	0.08125	0.31	0.000291	1.5	0.000008	10.2	1201±9	2.794	0.8	0.260	0.2	1.565	2.0	0.141	2.0
528-95**	Stage 2 Ur	0.08170	0.34	0.000229	1.7	0.000010	13.4	1068±9	3.224	0.8	0.299	0.2	1.730	2.0	0.154	2.0
211-136**	Stage 3 Ur	0.06420	0.67	0.000520	1.8	0.000013	27.5	722±19	0.6835	1.1	0.0797	0.8	0.584	5.0	0.0662	5.0
211-136	Cof	0.05180	0.66	0.004739	0.6	0.000111	9.0	286±19	0.3075	1.1	0.0450	0.6	0.334	5.0	0.0458	5.0
211-136	Cof	0.05112	0.58	0.005841	1.5	0.000131	5.4	260±17	0.3058	1.6	0.0448	1.1	0.333	5.0	0.0457	5.0
211-136	Cof	0.05169	0.67	0.006371	0.9	0.000108	6.1	282±19	0.3102	1.2	0.0452	0.8	0.336	5.0	0.0460	5.0
211-136	CaU	0.05191	1.4	0.004476	2.0	0.000087	9.4	291±39	0.3154	1.6	0.0457	0.7	0.340	5.0	0.0464	5.0
211-136	CaU	0.05014	1.0	0.003051	3.0	0.000056	12.1	220±29	0.2755	1.3	0.0416	0.5	0.309	5.0	0.0437	5.0
211-136	CaU	0.05161	0.3	0.007450	1.2	0.000122	12.8	279±9	0.3131	0.9	0.0458	0.7	0.338	5.0	0.0464	5.0
211-136	CaU	0.05009	1.3	0.001450	1.9	0.000039	14.4	218±37	0.2881	1.5	0.0436	0.5	0.319	5.0	0.0450	5.0
528-95	Stage 2 Ur	0.07114	0.22	0.001029	1.4	0.000018	20.8	931±6	1.080	0.9	0.114	0.8	0.805	2.0	0.083	2.0
528-95**	Stage 2 Ur	0.08125	0.31	0.000291	1.5	0.000008	10.2	1201±9	2.794	0.8	0.260	0.2	1.565	2.0	0.141	2.0
528-95**	Stage 2 Ur	0.08170	0.34	0.000229	1.7	0.000010	13.4	1068±9	3.224	0.8	0.299	0.2	1.730	2.0	0.154	2.0

McArthur River

204-503	Stage 1 Ur	0.08422	0.35	0.000143	2.1	0.000004	19.9	1274±10	4.263	0.9	0.383	0.4	2.104	2.0	0.181	2.0
204-503	Stage 1 Ur	0.08346	0.21	0.000151	2.6	0.000004	22.5	1256±6	4.264	0.5	0.383	0.1	2.104	2.0	0.181	2.0
204-503	Stage 1 Ur	0.08310	0.24	0.000120	2.1	0.000005	17.0	1247±7	4.237	0.4	0.386	0.1	2.095	2.0	0.182	2.0
204-503	Stage 1 Ur	0.08266	0.20	0.000187	2.5	0.000004	15.5	1236±6	4.185	0.4	0.381	0.1	2.077	2.0	0.180	2.0
204-503	Stage 1 Ur	0.08224	0.30	0.000169	1.6	0.000005	18.3	1226±9	3.924	0.5	0.360	0.3	1.985	2.0	0.174	2.0
204-503	Stage 1 Ur	0.08053	0.30	0.000139	1.0	0.000007	21.2	1183±9	3.592	1.1	0.335	0.8	1.866	2.0	0.166	2.0
204-503**	Stage 1 Ur	0.08334	0.22	0.000299	1.0	0.000008	17.2	1253±3	3.786	0.8	0.341	0.3	1.936	2.0	0.168	2.0
204-503	Stage 1 Ur	0.08377	0.24	0.000309	2.1	0.000007	16.7	1263±3	4.237	0.5	0.379	0.1	2.095	2.0	0.180	2.0
204-503	Stage 1 Ur	0.08423	0.36	0.000131	1.8	0.000004	12.2	1274±5	4.334	0.6	0.390	0.3	2.128	2.0	0.183	2.0
204-503**	Stage 1 Ur	0.07994	0.20	0.000121	2.2	0.000010	12.7	1168±6	3.934	0.6	0.374	0.3	1.989	2.0	0.178	2.0
236-515	Stage 1 Ur	0.07267	0.35	0.002192	1.4	0.000046	4.9	974±10	2.427	0.9	0.251	0.7	1.418	2.5	0.138	2.5
236-515	Stage 1 Ur	0.07352	0.19	0.002567	0.9	0.000061	4.7	998±6	2.462	1.1	0.255	0.7	1.432	2.5	0.139	2.5
236-515	Stage 1 Ur	0.07194	0.36	0.002675	1.3	0.000052	5.5	954±10	2.334	0.8	0.246	0.4	1.380	2.5	0.136	2.5
236-515**	Stage 3 Ur	0.06519	0.43	0.000282	1.7	0.000012	9.4	745±12	2.165	0.7	0.254	0.2	1.309	2.5	0.139	2.5
236-515**	Stage 3 Ur	0.07326	0.28	0.001285	1.0	0.000031	11.5	991±8	2.963	0.6	0.306	0.4	1.631	2.5	0.157	2.5
236-515	Stage 3 Ur	0.06604	0.21	0.000110	2.1	0.000007	17.5	780±6	2.479	0.5	0.287	0.3	1.439	2.5	0.150	2.5
236-515	Stage 3 Ur	0.06639	0.35	0.000105	2.2	0.000005	14.5	791±3	2.540	0.8	0.290	0.7	1.464	2.5	0.151	2.5
236-515**	Stage 3 Ur	0.06984	0.27	0.001155	1.5	0.000028	4.6	894±8	2.505	0.4	0.271	0.4	1.450	2.5	0.145	2.5
236-515**	Stage 3 Ur	0.06728	0.12	0.000077	3.1	0.000006	12.2	818±3	2.627	0.8	0.293	0.5	1.499	2.5	0.152	2.5
236-515**	Stage 3 Ur	0.06915	0.36	0.001664	0.6	0.000040	5.7	873±10	2.195	0.9	0.239	0.9	1.322	2.5	0.134	2.5
236-511	Stage 2 Ur	0.08247	0.48	0.000556	1.3	0.000008	16.1	1231±14	1.696	1.5	0.156	1.0	1.104	2.2	0.102	2.2
236-511	Stage 2 Ur	0.08203	0.55	0.000602	1.8	0.000010	14.4	1221±16	1.392	2.2	0.127	1.5	0.961	2.2	0.089	2.2
236-511**	Stage 2 Ur	0.07421	0.99	0.005522	1.1	0.000131	13.8	1017±28	0.125	1.5	0.013	1.0	0.178	2.2	0.021	2.2
236-511	Stage 2 Ur	0.07736	1.4	0.002787	4.8	0.000094	24.2	1101±39	0.085	2.2	0.008	1.5	0.136	2.2	0.016	2.2
236-511	Stage 2 Ur	0.07870	0.22	0.000280	2.3	0.000007	18.6	1136±6	3.260	1.0	0.315	0.7	1.743	2.2	0.160	2.2
236-511**	Stage 2 Ur	0.07926	0.12	0.000231	1.3	0.000007	18.5	1151±3	3.373	1.0	0.320	1.0	1.786	2.2	0.161	2.2
236-511	Stage 2 Ur	0.07763	0.39	0.000360	1.1	0.000008	6.2	1108±11	3.161	1.1	0.305	0.7	1.706	2.2	0.156	2.2

Abbreviations: Ur: uraninite, Cof: coffinite, CaU: calciouranoite, DDH: diamond drill hole.
* Values of ratios corrected using equations [1] and [2] from text. ** Data not used in concordia plots. See text for discussion.

growth, and variable $^{207}Pb/^{206}Pb$ ages (1359 to 218 Ma, Table 4). Higher-reflectance regions in these samples give older $^{207}Pb/^{206}Pb$ ages and are interpreted to be remnant grains of earlier-formed uraninite that were not completely overprinted by subsequent fluids (Figs. 8a, b). The composite nature of the uraninite suggests that fluids have recrystallized older generations of uraninite, partially resetting the Pb isotope systematics of the precursor mineral. Si- and Ca-rich uranium minerals have the youngest $^{207}Pb/^{206}Pb$ ages, ranging from 291 to 218 Ma.

Despite the wide range in $^{207}Pb/^{206}Pb$ ages in the Athabasca deposits (Table 4), there are distinct clusters at ~1350, 1250, 1000, 750 and 250 Ma, which correspond to the global tectonic and thermal events that have affected the region (Fig. 9), such as the accretion of the supercontinent Nena (~1.5 Ga), the thermal event that emplaced the Mackenzie dike swarm proximal to these deposits at ~1.3 Ga (Lecheminant & Heaman 1989), the Grenvillian Orogeny (~1100 Ma, Mallard & Rogers 1997), which occurred to the southeast of the Athabasca Basin, and the accretion (~1 Ga) of the supercontinent Rodinia (Young 1992, Kotzer *et al.* 1992, Li *et al.* 1996, Hoffman 1991, Kyser 2000, Kyser *et al.* 2000), the breakup (~900 to 700 Ma) of Rodinia (Young 1992, Li *et al.* 1996, Hoffman 1991, Kyser 2000, Kyser *et al.* 2000), and the breakup of the supercontinent Pangea (~250 Ma: Rogers 1996). Therefore, each stage of uranium mineralization may represent a new stage of mineral growth from a uranium-bearing fluid or local recrystallization and isotopic resetting of previously existing minerals by fluid migration associated with a specific global tectonic event.

The complex textures observed within a single thin section (Figs. 8a, b) are generally visible using backscattered electron (BSE) imaging, whereas during SIMS analysis, transmitted light is used to navigate across samples. Therefore, samples analyzed by SIMS for their U–Pb isotopic composition were re-examined using BSE. Cases in which the ion beam sampled more than one generation of uraninite or impinged the sample near a fracture (Fig. 8c) were eliminated from the data set used for the concordia plots.

Figures 10a and b show concordia plots of the U–Pb data from stage-1 uraninite from the Sue zone and McArthur River deposits, respectively (Table 4). An upper intercept of 1486 ± 9 Ma and lower intercept of 458 ± 18 Ma were obtained for the Sue Zone, with a mean standard weighted deviation (MSWD) of 1.7 for 18 points, whereas an upper intercept of 1519 ± 22 Ma and lower intercept of 643 ± 20 Ma were obtained for McArthur River with an MSWD of 1.2 for 11 points. The ages obtained from these regressions are some the oldest ages ever obtained for the Canadian unconformity-type deposits; they are interpreted to represent the minimum age of mineralization. These ages correspond to the age of one of the magnetization events (B-type magnetization, 1600–1450 Ma) in the Athabasca basin (Kotzer *et al.* 1992).

Figures 10c and d show concordia plots of the U–Pb data from stage-2 uraninite from both the Sue Zone and McArthur River deposits, respectively (Table 4). Regression of the points gave upper intercepts of 1126 ± 73 and 1189 ± 10 Ma, and lower intercepts of 196 ± 85 and 48 ± 15 Ma, respectively. The ages obtained from the regressions are also interpreted to represent the minimum age of mineralization and correspond to the Grenvillian Orogeny (~1100 Ma, Mallard & Rogers 1997), which occurred to the southeast of the Athabasca Basin, and the accretion (~1 Ga) of the supercontinent Rodinia (Young 1992, Kotzer *et al.* 1992, Li *et al.* 1996, Hoffman 1991, Kyser 2000, Kyser *et al.* 2000).

Ca–U-rich minerals and coffinite from the Sue Zone plot on concordia at 283 ± 20 Ma (Table 4, Fig. 10e). These data pertain to samples that contain fine intergrowths of Ca–U-rich minerals and coffinite (Fig. 8b), which generally have low contents of uranium. This age corresponds to the assemblage of the supercontinent Pangea (~300 Ma) near the end of the Paleozoic (Rogers 1996, Kyser *et al.* 2000). Stage-3 uraninite from the McArthur River deposit also plots on or near concordia

TABLE 5. ION-MICROPROBE DATA ON OXIDE RATIO IN URANINITE STANDARDS

Sample	$^{206}Pb^+/^{238}U^+$ SIMS	error (%)	UO^+/U^+ SIMS	error (%)	UO_2^+/U^+ SIMS	error (%)
Sue 129	0.4714	0.2	3.952	0.1	1.0200	0.1
	0.5086	0.2	3.828	0.1	0.9724	0.1
	0.4702	0.2	3.749	0.1	0.9470	0.1
	0.4836	0.2	3.441	0.1	0.7458	0.1
	0.5094	0.2	3.488	0.1	0.7620	0.1
Mc 503	0.4289	0.2	3.575	0.1	0.8129	0.1
	0.4281	0.2	3.597	0.1	0.8244	0.1
Mc 515	0.2946	0.3	3.872	0.1	0.9942	0.1
	0.2888	0.3	3.820	0.1	0.9783	0.1
	0.2950	0.0	3.534	0.1	0.7981	0.1
LAMNH-30222	0.0535	1.9	2.686	0.1	0.9632	0.1
	0.0566	1.8	2.705	0.1	0.9744	0.2
	0.0582	1.7	2.379	0.1	0.4570	0.1

Errors are expressed as 2σ in all cases. See the text for conditions of analysis.

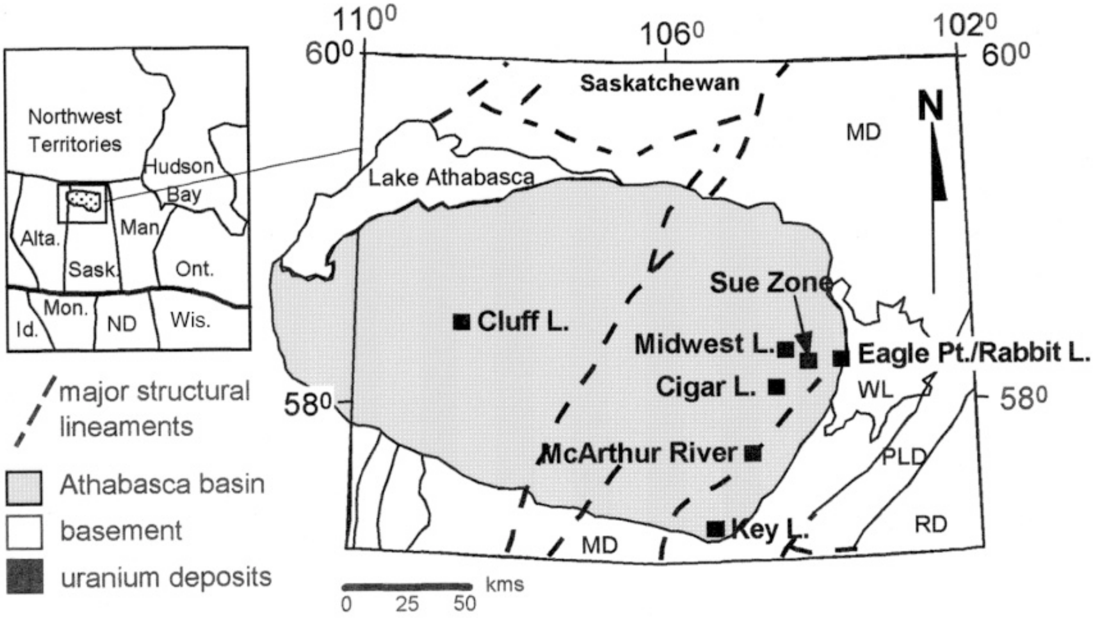

FIG. 7. Map showing the extent of the Athabasca Basin, location of the uranium deposits, and major lithostructural domains in the crystalline basement of Saskatchewan (modified from Hoeve & Sibbald 1978). Abbreviations: MD: Mudjatik Domain; WD: Wollaston Domain; PLD: Peter Lake Domain; RD: Rottenstone Domain; and WL: Wollaston Lake; R: River; L: Lake.

at 910 ± 20 Ma (Fig. 10f), which corresponds with the breakup (~900 to 700 Ma) of Rodinia and the age of C-type magnetization (~950 Ma) in the Athabasca Basin (Kotzer *et al.* 1992).

The concordia results define well-correlated arrays, compared to the data obtained from mineral separation and techniques of thermal ionization mass spectrometry (Cumming & Krstic 1992). These Pb–Pb and U–Pb ages correlate with large-scale diagenetic fluid-circulation events that formed these deposits, affected the entire Athabasca basin, and led to significant thermal, orogenic and tectonic events. Prior to *in situ* analyses, evidence for such events was obscured by the wide variability in the data obtained by micro-drilling and conventional isotopic analyses. This detailed chronology, which was previously unavailable, indicates that Pb–Pb and U–Pb isotope systematics of these deposits are sensitive to fluid-circulation events, recording the timing of fluid interaction, and providing crucial information necessary to unravel the history of fluids in these deposits.

CONCLUSIONS

1. A robust method for obtaining accurate U–Pb isotopic analysis of uranium-rich minerals by SIMS has been developed. An ion-yield normalizing coefficient (αSIMS), which is the ratio of the "true" values for ^{206}Pb/^{238}U and ^{207}Pb/^{235}U *versus* the ^{206}Pb^{+}/^{238}U^{+} and ^{207}Pb^{+}/^{235}U^{+} values determined by SIMS, was calculated for a suite of uraninite standards that covered a range of U and Pb compositions.

2. The αSIMS coefficients vary as a function of wt% PbO and primary ion-beam current. Therefore, keeping the current of the primary ion-beam constant, an empirical mass-bias model was developed, which included two calibration curves that define the relationship between the ^{206}Pb^{+}/^{238}U^{+} and ^{207}Pb^{+}/^{235}U^{+} values measured by SIMS *versus* the "true" ^{206}Pb/^{238}U and ^{207}Pb/^{235}U values.

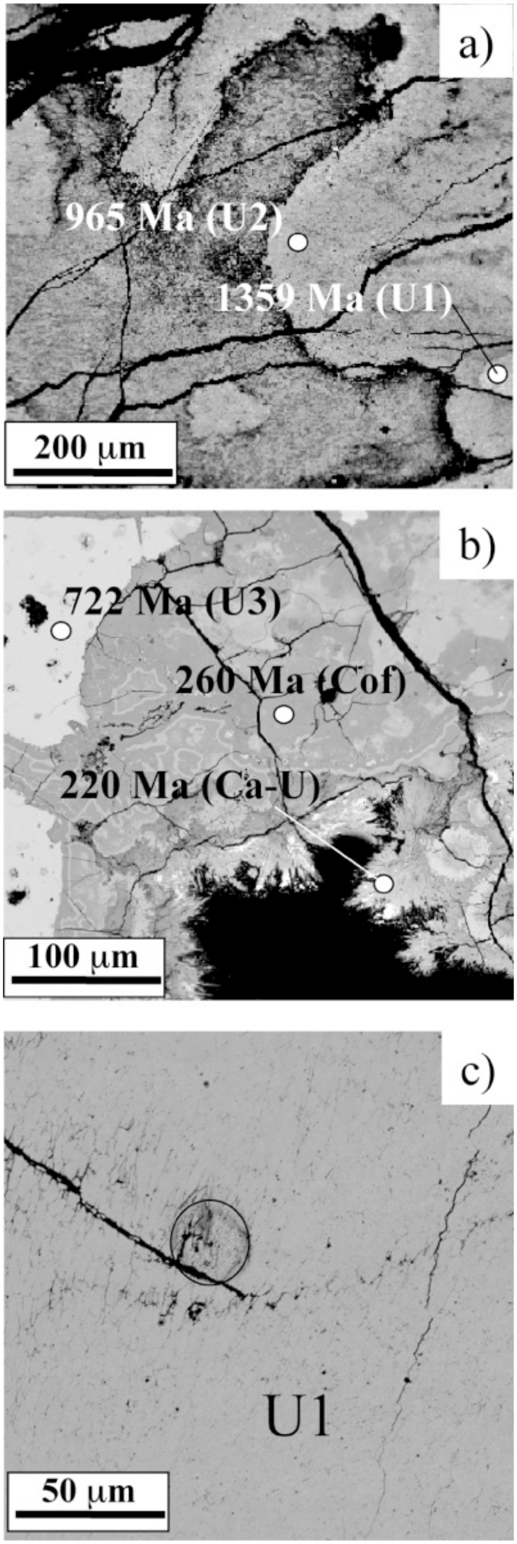

FIG. 8. (a) Back-scattered electron image of uraninite from the Sue Zone uranium deposit (sample 528–95), Athabasca Basin. Bright patches represent remnant early-stage uraninite that was not completely recrystallized. Also shown are ^{207}Pb/^{206}Pb ages calculated from *in situ* microanalysis obtained by ion microprobe. (b) Back-scattered electron image of uraninite (U), coffinite (Cof) and calcium uranyl oxide hydrate minerals (Ca–U) from the Sue Zone uranium deposit (sample 211–136). Also shown are the spots that were analyzed by ion microprobe and the calculated ^{207}Pb/^{206}Pb ages. (c) Back-scattered electron image of an ion-microprobe pit that overlaps a crack in a sample of uraninite (204–503) from the McArthur River uranium deposit, Athabasca Basin. The data obtained from this spot were not used in the concordia diagrams.

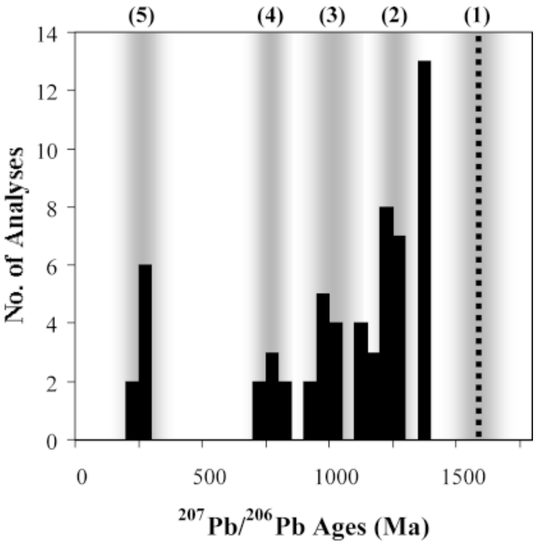

FIG. 9. Distribution of ^{207}Pb/^{206}Pb ages of uranium minerals relative to major tectonic events that have affected the Athabasca Basin region. The black dashed line represents the U–Pb age of formation for the Athabasca uranium deposits (~1.5 Ga), and the numbers in parentheses mark the following tectonic events (1) Accretion of Nena (~1.5 Ga), (2) thermal event leading to the emplacement of the Mackenzie dike swarm (~1.3 Ga), (3) The Grenvillian Orogeny (1.1 Ga) and the accretion of Rodinia (~1.0 Ga), (4) the breakup of Rodinia (0.9–0.7 Ga), and (5) the breakup of Pangea (~250 Ma). These deposits represent one of the few areas in the world that have preserved a nearly complete neotectonic record of the continents over the past 1.5 Ga. Data from Table 4.

3. The *in situ* U–Pb ages calculated from data obtained by SIMS are some the oldest ages ever reported for unconformity-type uranium deposits. These ages, as well as the ages obtained for stage-2 and -3 uraninite, indicate the timing and nature of the recrystallization events. Prior to the *in situ* analyses, such information was obscured owing to the wide variability in the data obtained by micro-drilling and TIMS analyses.

4. The Pb–Pb and U–Pb ages obtained in this study (~1500, 1150, 900 and 280 Ma) are related to either large-scale events involving the circulation of diagenetic fluid that formed these deposits and affected the entire Athabasca basin (~1500 Ma), or the migration of fluid related to major tectonic, thermal and orogenic events such as the Mackenzie dyke swarm (~1300 Ma), the Grenvillian Orogeny (~1100 Ma), the accretion and breakup of Rhodinia (~1000 and 700 Ma, respectively), and the assemblage of Pangea (~300 Ma).

ACKNOWLEDGEMENTS

The research was sponsored by the Division of Chemical Sciences, Geosciences, and Biosciences, Office of Basic Energy Sciences, U.S. Department of Energy, under contract DE–AC05–00OR22725 with Oak Ridge National Laboratory, managed and operated by UT-Battelle, LLC. The comments of the two reviewers and Prof. Robert F. Martin have greatly benefitted this manuscript.

REFERENCES

ANDERSON, C.A. & HINTHORNE, J.R. (1972): U, Th, Pb and REE abundances and ^{207}Pb/^{206}Pb ages of individual minerals in returned lunar material by ion-microprobe mass analysis. *Earth Planet. Sci. Lett.* **14**, 195-200.

BERMAN, R.M. (1957): The role of lead and excess oxygen in uraninite. *Am. Mineral.* **42**, 705-731.

CATHELINEAU, M., BOIRON, M.C., HOLLIGER, P. & POTY, B. (1990): Metallogenesis of the French part of the Variscan orogen. II. Time–space relationships between U, Au and Sn–W ore deposition and geodynamic events – mineralogical and U–Pb data. *Tectonophys.* **177**, 59-79.

CLAOUÉ-LONG, J.C., COMPSTON, W., ROBERTS, J. & FANNING, C.M. (1995): Two Carboniferous ages: a comparison of SHRIMP zircon dating with conventional zircon ages and ^{40}Ar/^{39}Ar analysis. *In* Geochronology, Time Scales and Global Stratigraphic Correlation (W.A. Berggren, D.V. Kent, M.-P. Aubry & J. Hardenbol, eds.). *SEPM, Spec. Publ.* **4**, 3-21.

CUMMING, G.L. & KRSTIC, D. (1992): The age of unconformity-related uranium mineralization in the Athabasca Basin, northern Saskatchewan. *Can. J. Earth Sci.* **29**, 1623-1639.

EVINS, Z.L., SUNDE, T., SCHÖBERG, H. & FAYEK, M. (2001): U and Pb isotope calibration of uraninite and galena standards for SIMS. *SKB Tech. Rep.* **TR-01-35**.

FAYEK, M., HARRISON, T.M., EWING, R.C., GROVE, M. & COATH, C.D. (2002): O and Pb isotopic analyses of uranium minerals by ion microprobe and U–Pb ages from the Cigar Lake deposit. *Chem. Geol.* **185**, 205-225.

________, ________, GROVE, M. & COATH, C.D. (2000): A rapid *in situ* method for determining the ages of uranium oxide minerals: evolution of the Cigar Lake deposit, Athabasca Basin. *Int. Geol. Rev.* **42**, 163-171.

________, ________, ________, ________ & EWING, R.C. (2001): In situ stable isotopic analyses of multiple generations of cementation associated with a petroleum reservoir, North Coles Levee, San Joaquin Basin, California. *J. Sedim. Res.* **71**, 444-485.

________, JANECZEK, J. & EWING, P.C. (1997b): Mineral chemistry and oxygen isotopic analyses of uraninite, pitchblende and uranium alteration minerals from the Cigar

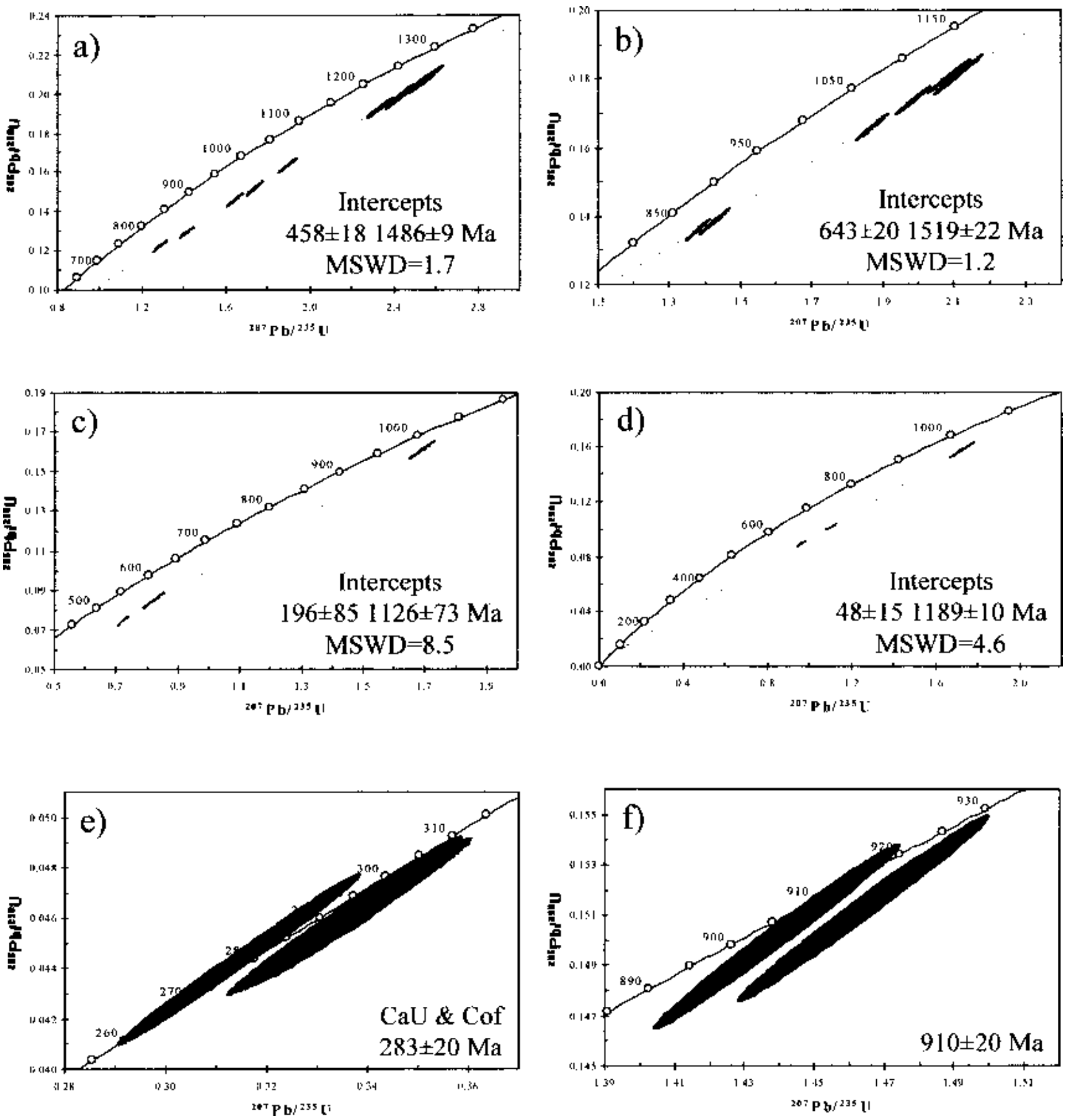

FIG. 10. U–Pb results from *in situ* isotopic analyses of (a) stage-1 uraninite from the Sue Zone, (b) stage-1 uraninite from the McArthur River deposit, (c) and (d) stage-2 uraninite from the Sue Zone and McArthur River deposits, (e) coffinite and Ca–U-rich phases from the Sue Zone, and (f) stage-3 uraninite from the McArthur River deposit. The data are reported in Table 4.

Lake deposit, Saskatchewan, Canada. *Appl. Geochem.* **12**, 549-565.

________ & KYSER, T.K. (1997): Characterization of multiple fluid events and rare-earth-element mobility associated with formation of unconformity-type uranium deposits in the Athabasca Basin, Saskatchewan. *Can. Mineral.* **35**, 627-658.

________, ________, EWING, R.C. & MILLER, M.L. (1997a): Uraninite–water interaction in an oxidizing environment. *Mater. Res. Soc., Symp. Proc.* **465**, 1201-1208.

FOUREL, F., LANCELOT, J.R., ALLÈGRE, C.J. & DUPRÉ, B. (1988): Isotopic analyses of uraniferous minerals by both U–Pb and Sm–Nd methods. *Chem. Geol.* **70**, 134 (abstr.).

Hoeve, J., Cumming, G.L., Baadsgaard, H. & Morton, R.D. (1985): Geochronology of uranium metallogenesis in Saskatchewan. *In* Geology of Uranium Geposits (T.I.I. Sibbald & W. Petruk, eds.). *Can. Inst. Mining Metall., Spec. Vol.* **32**, 56-63.

________ & Sibbald, T.I.I. (1978): On the genesis of Rabbit Lake and other unconformity-type uranium deposits in northern Saskatchewan, Canada. *Econ. Geol.* **73**, 1450-1473.

Hoffman, P.F. (1991): Did the breakout of Laurentia turn Gondwana inside-out? *Science* **252**, 1409-1412.

Holliger, P. (1988): Ages U–Pb définis in-situ sur les oxydes d'uranium à l'analyseur ionique: méthodologie et conséquences géochimiques. *C.R. Acad. Sci. Paris, Sér. 2*, **307**, 367-373.

________ (1991): SIMS isotope analyses of U and Pb in uranium oxides: geological and nuclear applications. *8th Int. SIMS Conf., Proc.*, 719-722.

________ (1994): SIMS studies on the Oklo natural fission reactors. *9th Int. SIMS Conf., Proc.*, 906-910.

________ & Cathelineau, M. (1986): Le chronomètre U–Pb en milieu uranifère: application aux gisements hydrothermaux d'uranium liés spatialement au batholithe de Mortagne (Vendée, France). *Chron. Rech. Min.* **485**, 33-43.

________ & ________ (1987): Ion-microprobe lead isotopic measurements on U-ore minerals: application for in-situ determined Pb–Pb apparent ages. *Terra Cognita* **7**, 230.

________ & ________ (1988): In situ U–Pb age determination by secondary ion mass sepctrometry. *Chem. Geol.* **70**, 173 (abstr.).

Kotzer, T.G. & Kyser, T.K. (1993): O, U and Pb isotopic and chemical variations in uraninite: implications for determining the temporal and fluid history of ancient terrains. *Am. Mineral.* **78**, 1262-1274.

________ & ________ (1995): Petrogenesis of the Proterozoic Athabasca Basin, northern Saskatchewan, Canada, and its relation to diagenesis, hydrothermal uranium mineralization and paleohydrogeology. *Chem. Geol.* **120**, 45-89.

________, ________ & Irving, E. (1992): Paleomagnetism and the evolution of the fluids in the Proterozoic Athabasca Basin, northern Saskatchewan, Canada. *Can. J. Earth Sci.* **29**, 1474-1491.

Kyser, T.K. (2000): Controls on fluids and basins. *In* Fluids and Basin Evolution (T.K. Kyser, ed.). *Mineral. Assoc. Can., Short Course* **28**, 1-18.

________, Hiatt, E.E., Renac, C., Durocher, K., Holk, G. & Deckart, K. (2000): Diagenetic fluids in paleo- and meso-Proterozoic sedimentary basins and their implications for long protracted fluid histories. *In* Fluids and Basin Evolution (T.K. Kyser, ed.). *Mineral. Assoc. Can., Short Course* **28**, 225-262.

Lecheminant, A.N. & Heaman, L.M. (1989): Mackenzie igneous events, Canada: Middle Proterozoic hotspot magmatism associated with ocean opening. *Earth Planet. Sci. Lett.* **96**, 38-48.

Li, Z.X., Zhang, L. & Powel, C. (1996): Positions of the East Asian cratons in the Neoproterozoic supercontinent Rodinia. *Aust. J. Earth. Sci.* **43**, 593-604.

Ludwig, K.R. (1993): ISOPLOT. A plotting and regression program for radiogenic-isotope data. *U.S. Geol. Surv., Open File Rep.* **91-445**.

Lyon, I.C., Saxton, J.M. & Turner, G. (1994): Isotopic fractionation in secondary ionization mass spectrometry. *Rapid Commun. Mass Spectrom.* **8**, 837-843.

MacDonald, R. (1987): Update on the Precambrian geology and domainal classification of northern Saskatchewan. *In* Summary of Investigations 1987. *Saskatchewan Geol. Surv., Misc. Rep.* **87-4**, 87-104.

Mallard, L.D. & Rogers, J.J.W. (1997): Relationship of Avalonian and Cadomian terranes to Grenville and Pan-African events. *J. Geodynamics* **23**, 197-221.

Meddaugh, W.S. (1983): *Age and Origin of Uraninite in the Elliot Lake, Ontario Uranium Ores.* Ph.D. thesis, Harvard Univ., Cambridge, Massachusetts.

Meyer, C., Williams, I.S. & Compston, W. (1996): U–Pb ages for lunar zircons: evidence for a prolonged period of granophyre formation from 4.32 to 3.88 Ga. *Meteor. Planet. Sci.* **31**, 370-387.

Pagel, M., Poty, B. & Sheppard, S.M.F. (1980): Contributions to some Saskatchewan uranium deposits mainly from fluid inclusions and isotopic data. *In* Uranium in the Pine Creek Geosyncline (S. Ferguson & A.B. Goleby, eds.). *IAEA* (*Vienna*), **STI/PUB/555**, 639-654.

Ramaekers, P. (1981): Hudsonian and Helikian basins of the Athabasca Region, northern Saskatchewan. *In* Proterozoic Basins of Canada (F.H.A. Campbell, ed.). *Geol. Surv. Can., Pap.* **81-10**, 219-233.

Reed, S.J.B. (1989): Ion-microprobe analysis – a review of geological applications. *Mineral. Mag.* **53**, 3-24.

Riciputi, L.R., Paterson, B.A. & Ripperdan, R.L. (1998): Measurement of light stable isotope ratios by SIMS: matrix effects for oxygen, carbon, and sulfur isotopes in minerals. *Int. J. Mass Spectrom.* **178**, 81-112.

Rogers, J.J.W. (1996): A history of continents in the past three billion years. *J. Geol.* **104**, 91-107.

Schroeer, J.M., Rhodin, T.N. & Bradley, R.C. (1973): A quantum-mechanical model for the ionization and excitation of atoms during sputtering. *Surface Sci.* **34**, 571-580.

SHIMIZU, N. & HART, S.R. (1982): Applications of the ion-microprobe to geochemistry and cosmochemistry. *Annu. Rev. Earth Planet. Sci.* **10**, 483-526.

SIGMUND, P. (1969): Theory of sputtering. I. Sputtering yield of amorphous and polycrystalline targets. *Phys. Rev*. **184**, 383-416.

WILLIAMS, I.S. (1998): U–Th–Pb geochronology by ion microprobe. *In* Applications of Micronanalytical Techniques to Understanding Mineralizing Processes (M.A. McKibben, W.C. Shanks, III & W.I. Ridley, eds.). *Rev. Econ. Geol*. **7**, 1-35.

________, BUICK, I.S. & CARTWRIGHT, I. (1996): An extended episode of early Mesoproterozoic metamorphic fluid flow in the Reynolds Range, central Australia. *J. Metamorh. Geol.* **14**, 29-47.

WILLIAMS, P. (1979): The sputtering process and sputtered ion emission. *Surface Sci*. **90**, 588-643.

________ (1988): Aspects of quantitative analysis using secondary ion microanalyser. *In* Secondary Ion Mass Spectrometry, SIMS VI (A. Benninghoven, A.M. Huber & H.W. Werner, eds.). John Wiley & Sons, Chichester, U.K. (261-268).

YOUNG, G.M. (1992): Late Proterozoic stratigraphy and the Canada–Australia connection. *Geology* **20**, 215-218.

YU, M.L. & LANG, N.D. (1986): Mechanisms of atomic ion emission during sputtering. *Nucl. Instrum. Methods* **B14**, 403-413.

Received February 1, 2002, revised manuscript accepted November 11, 2002.